12th International Symposium on Turbulence and Shear Flow Phenomena (TSFP12)
Osaka, Japan (Online), July 19-22, 2022

NUMERICAL STUDY OF TURBULENT RESISTANCE REDUCTION EFFECT BY STAGGERED SUPERHYDROPHOBIC SURFACE

Daito Hirata, Hiroya Mamori,Takeshi Miyazaki
Department of Mechanical and Intelligent Systems Engineering
The University of Electro-Communications
1-5-1 Chofugaoka, Chofu, Tokyo, 182-8585, Japan
mamori@uec.ac.jp

ABSTRACT

Direct numerical simulations of the turbulent channel flow with superhydrophobic surfaces (SHS) are performed. We employed a staggered type of the SHS and confirmed a drag reduction effect and an increase of a mean streamwise velocity, while the reduction rate is lower than that of the straight type. In addition, we investigate the influence of particle adhesion on the drag reduction effect. The particle adhesion decreases the drag reduction effect by the SHS. The number of adhered particles on the staggered SHS is smaller than that of the streamwise straight SHS. Therefore, we expect the staggered SHS to maintain the drag reduction effect longer than the streamwise straight SHS.

INTRODUCTION

In turbulent flows, the skin-friction drag accounts for a substantial proportion of the total drag. The superhydrophobic surface (referred to as the SHS, hereafter) decreases the skin-friction drag and has been widely studied (e.g. Daniello, *et al.*, 2009; Choi and Kim, 2006). The friction drag reduction is obtained due to the slip velocity. The slip velocity occurs at the interface between the trapped air into the micro-groove and the working fluid.

To simulate the turbulent flow over the SHS, the SHS is represented by combining the no-slip and slip area. Hasegawa *et al.*(2011) performed direct numerical simulations (DNS) of turbulent channel flows with straight and sinuous types of the SHS and found the increase of the bulk mean velocity. Michael *et al.*(2009) performed the DNS of turbulent channel flow to investigate the effects of width and gap of the slip area of the straight type of the SHS on the drag reduction effect. Watanabe *et al.*(2017) investigated the effect of the angle between the flow direction and the direction of the straight SHS on the bulk mean velocity using the DNS. When the direction of the SHS coincided with the flow direction, the bulk mean velocity increased up to 15%.

While the straight SHSs have been studied frequently, we investigate the effect of the staggered type of the SHS on the turbulent flow. Moreover, we investigate the influence of particle adhesion on the skin-friction drag. Since the SHS is expected to be used on ships as a practical application, the particles floating in the sea may adhere to the SHS and degrade the drag reduction rate. Therefore, the investigation of the effect of the particle adhesion on the skin-friction drag is required.

Accordingly, in this study, the numerical simulations of the turbulent channel flow with the straight and staggered types of the SHS are performed. The influence of the particle adhesion is investigated by evaluating the drag reduction rate, the flow statistics, and the number of adhered particles.

Table 1. Numerical conditions

Domain	$(L_x, L_y, L_z) = (2\pi, 2, 2\pi)$
Number of grids	$(N_x, N_y, N_z) = (256, 96, 256)$
Total slip area	50%
B_x	$L_x/10,\ L_x/2,\ L_x$
B_z	$L_z/10,\ L_z/2,\ L_z$

Direct Numerical Simulation

The DNS of the turbulent channel flow with or without the SHS is performed (Kim, *et al.*, 1987). The governing equations are continuity and the Navier-Stokes equations of the incompressible flow, as

$$\frac{\partial u_i}{\partial x_i} = 0 \tag{1}$$

$$\frac{\partial u_i}{\partial t} + u_j \frac{\partial u_i}{\partial x_j} = -\frac{\partial p}{\partial x_i} + \frac{1}{\mathrm{Re}_\tau} \frac{\partial^2 u_i}{\partial x_j^2} \tag{2}$$

Here, t is time and p is pressure. The streamwise, wall-normal, and spanwise coordinates are denoted by x, y, and z, and the corresponding velocities are u, v, and w, respectively. And x_i and u_i ($n = 1 \sim 3$) are interchangeably used. The driving force of the main flow is a constant pressure gradient condition, and the friction Reynolds number defined by the channel half-width and the wall-friction velocity is $\mathrm{Re}_\tau = u_\tau^* \delta^* / \nu^* = 180$. This corresponds to the bulk Reynolds number $\mathrm{Re_b} = 2u_b^* \delta^* / \nu^* = 5600$, where u_b^* is the bulk velocity and δ^* is the channel half-width. The asterisk means the dimensional variables.

The velocity and pressure are defined on the staggering grid system. The governing equations are discretized by using an energy-conserving second-order central difference method (Ham, *et al.*, 2002). As time advance, we employ the second-order Crank-Nicolson method for the viscous term and the memory-saving third-order Runge-Kutta method for the other

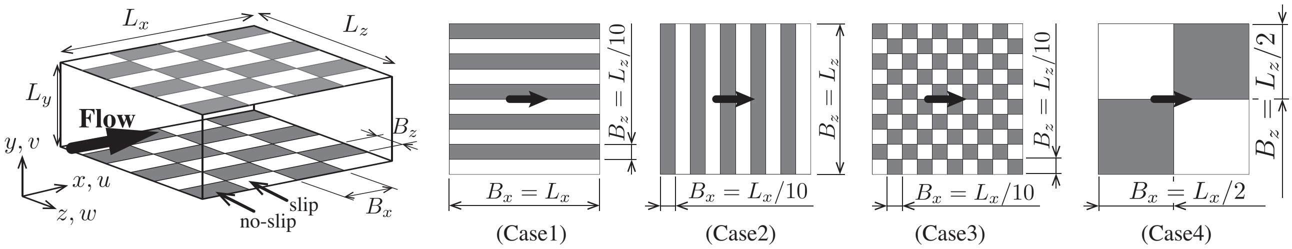

Figure 1. Schematic in the channel flow with the SHS.

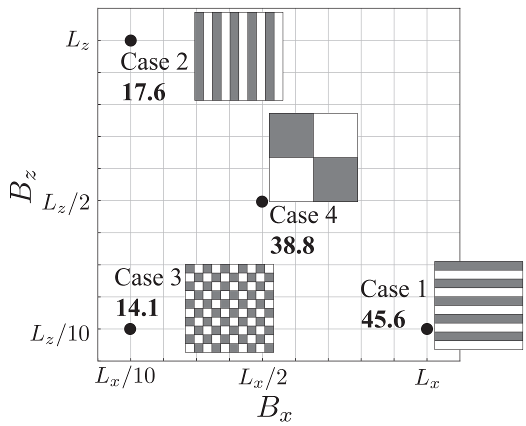

Figure 2. Drag reduction ratio for Cases 1 $\sim$ 4.

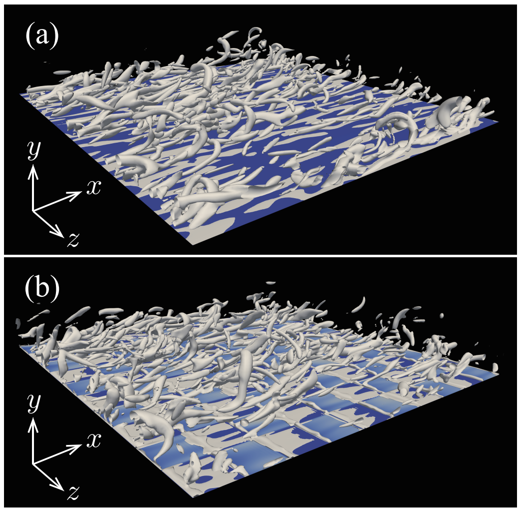

Figure 3. Schematic of the turbulent channel flow near the lower wall: (a) no-slip, (b) Case 3.

(Spalarta, *et al.*, 1991). Figure 1 shows a schematic of the channel flow with the SHS, and the numerical conditions are in Table 1.

The numerical condition is shown in Table 1. We imposed the periodic boundary condition in the x and z directions. The channel wall is the SHS represented by a combination of slip and no-slip conditions area alternately. In Fig. 1, the slip and no-slip areas are colored by white and black, respectively. The slip area is 50 percent of the entire wall surface, and a single slip area is defined by the streamwise length B_x and the spanwise length B_z. To maintain the symmetry of the flow field, the same SHS is installed on the upper and lower walls.

DRAG REDUCTION EFFECT

We perform the DNS of the turbulent channel flow with the SHS without the particles. Figure 2 shows the pattern of the SHS together with the drag reduction rate: Cases 1 and 2 are the straight types in the streamwise and spanwise directions, respectively; Cases 3 and 4 are the fine and coarse staggered type of the SHS, respectively. The drag reduction rate is defined as

$$R_D = \frac{C_{f0} - C_f}{C_{f0}} \tag{3}$$

Where C_f is the skin-friction coefficient. The subscript of zero means the no-slip case (without the particles). The drag reduction rate R_D is largest in Case 1 and low in Case 2. Furthermore, R_D in the finer staggered SHS of Case 3 is smaller than in the coarse SHS of Case 4. Figure 3 visualizes the turbulent vortical structures in the no-slip case and Case 3. The vortical structure is shown in white. In Case 3, the small vortical structure in the z direction was generated near the wall boundary between the no-slip and slip surfaces. There is no significant difference in the vortical structure above the wall between no-slip and Case 3.

Figure 4(a) shows the mean streamwise velocity. The streamwise velocity increased in all the as compared with the no-slip case. The velocity increased the most in Case 1, then in Case 4, Case 2, and Case 3. The result is consistent with Fig. 2, since the velocity increase corresponds to the decrease of the skin-friction drag under the constant pressure gradient condition. Figure 4(b) shows the streamwise velocity excluding the slip velocity on the wall $u|_{wall}$. A downward shift of velocity profile is observed in the buffer layer.

Figure 5(b) shows the Reynolds shear stress (referred to as the RSS, hereafter) in the area near the wall. The RSS in Case 2 is larger than that of the no-slip case. In contrast, in Cases 1 and 3-4, the negative RSS is found at $y^+ \leq 3$.

PARTICLE ADHESION

Subsequently, the influence of particle adhesion is discussed. We start simulations of the particle from the fully developed turbulent channel flow with the SHS. No particles are added during the simulation. The particles do not rotate, deform and interact with each other. The one-way coupling method is employed: the flow affects the particles by the Stokes resistance, but the particles do not affect the flow.

The equation of motion with the Stokes resistance of the particle is

$$m^* \frac{\partial \boldsymbol{v}_p^*}{\partial t} = -\frac{\pi}{2} \rho_f^* C_D r^{*2} \left| \boldsymbol{v}_p^* - \boldsymbol{v}_f^* \right| \left(\boldsymbol{v}_p^* - \boldsymbol{v}_f^* \right) \tag{4}$$

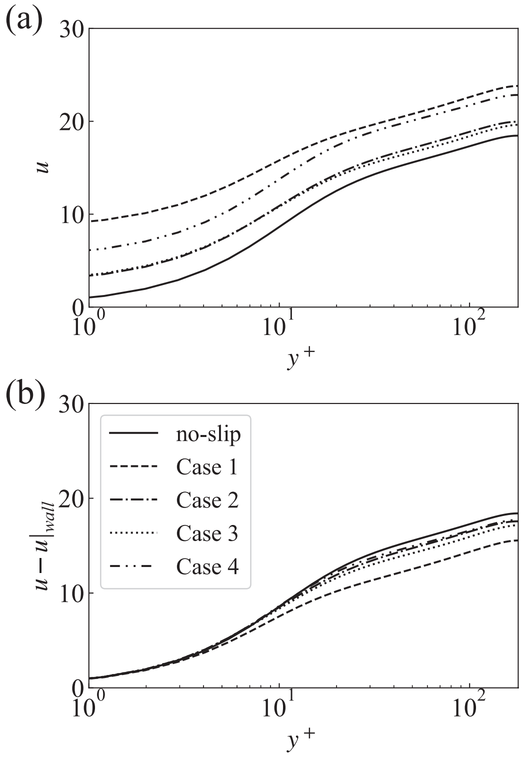

Figure 4. Mean streamwise velocity (a) u and (b) $u-u|_{wall}$.

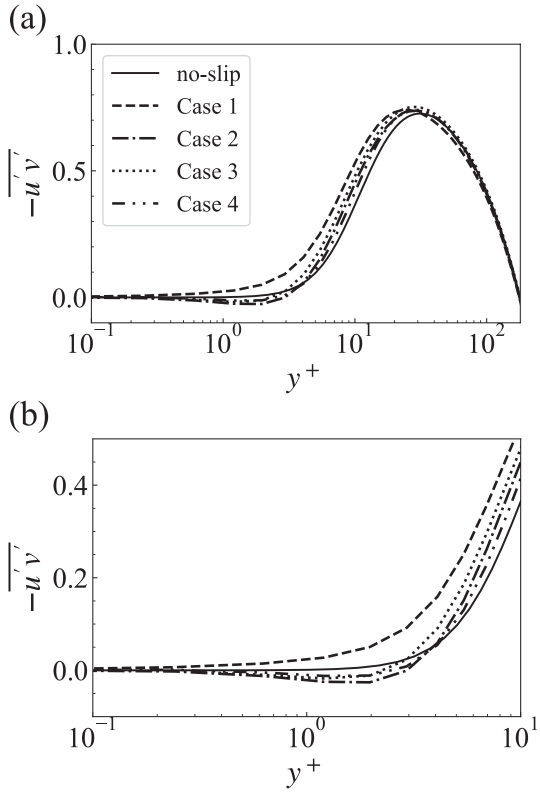

Figure 5. The Reynolds shear stress for different cases: (a) $0 < y^+ < 180$ and (b) zoom-up view of the near wall area.

Here, m is the mass of particles, r is the radius of the particle, ρ_p is the density ratio of the particles to the fluid, $\boldsymbol{v_p}$ is the particle velocity, $\boldsymbol{v_f}$ is the fluid velocity, and ρ_{pf} is the density of the fluid. The asterisk means dimensional quantities. The drag coefficient C_D is expected as,

$$\begin{cases} C_D = \dfrac{24}{\mathrm{Re}_p} & (\mathrm{Re}_p \leq 1) \\ C_D = \dfrac{24}{\mathrm{Re}_p}\left(1+0.15\mathrm{Re}_p^{0.678}\right) & (\mathrm{Re}_p \geq 1) \end{cases} \tag{5}$$

here, Re_p is a particle Reynolds number based on the particle diameter and the relative velocity between the flow and particles. In this simulation, the parameters are $\rho_{pf} = 3$ and $r = 2.5\times10^{-3}(r^+ = 0.45)$. The number of particles is 10,000. Therefore, the fraction of particles in the fluid is 0.008%. At the beginning of the simulation, the particles distribute randomly in the flow, and the local fluid velocity interpolates these velocities. To express the decrease of the SHS performance by the particle adhesion, we employ a simple model: the slip cell on the wall becomes the no-slip cell if the particle contacts. We compute the no-slip area by the adhesion based on the spherical surface of the particle.

Figure 6(a) shows the time trace of the bulk velocity considering the particle adhesion. The bulk velocity gradually decreased in Cases 1 and 4, while it is almost unchanged in Case 2 $\sim$ 3. The bulk velocity corresponds to the drag reduction rate. Figure 6(b) shows the time trace of the number of particles adhering to the SHS. The number of particles adhering to the SHS increased monotonically with time in all the cases. It implies that the particles are more likely to adhere to the streamwise straight type than the staggered type.

Figure 7 shows the accumulated adhered-particle on the wall at $0 < t < 80$ for all the cases. The white dot corresponds to the adhered particle. We found that the particles tend to adhere to the slip area.

In order to show the particle adhesion qualitatively, Fig. 8 shows the ratio of the local number of attachments to the total number of attachments. For Cases 1$\sim$3, the ratio is displayed in $2\pi/5\times2\pi/5$ since it is the smallest unit for the Case 3. We found that the particles tend to adhere to the slip area or the rear region of the slip area, as shown in Cases 1 and 2, respectively. In a fine staggered arrangement of Case 3, the particles adhere at the side area of the slip area, where the adhesion at the center area is little. In a coarse staggered arrangement of Case 4, the particles adhere uniformly on the slip area.

CONCLUSION

We obtain the significant drag reduction rate by the straight SHS in the streamwise direction, while the drag reduction rate by the staggered SHS is lower than that of the straight SHS. For the staggered SHS, the coarse SHS of Case 4 gives a more significant drag reduction rate than the finer staggered SHS of Case 3. Subsequently, we investigate the influence of particle adhesion on the SHS. The particle adhesion increases monotonically with time, and the number of the adhered particles in the staggered SHS is lower than that in the streamwise straight type. In the finer staggered SHS of Case 3, the decrement of the drag reduction rate and the number of the adhered particles are slight. Accordingly, the staggered SHS is robust for the drag reduction rate against the adhesion of the particles. The distribution of the particle adhesion is also investigated. In all the cases, the particles adhere to the slip area, and the distribution depends on the pattern of the SHS. In particular, in a fine staggered arrangement of Case 3, the particles tend to adhere to the side area of the slip area rather than the central area.

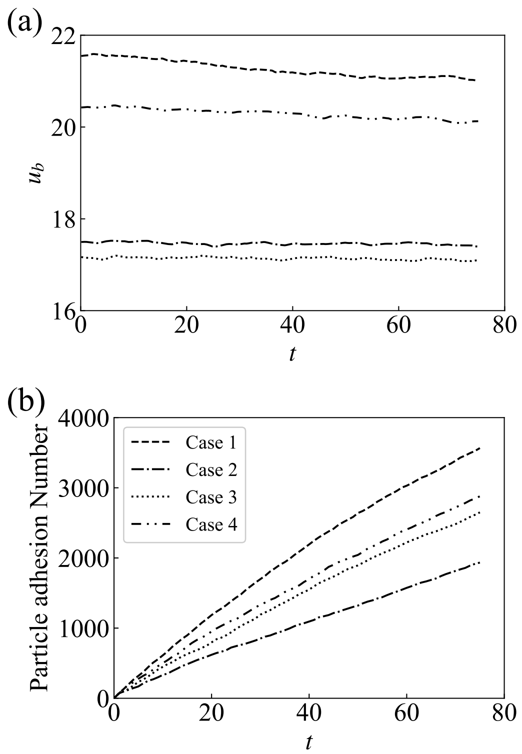

Figure 6. Time trace of (a) the bulk mean velocity and (b) the number of the particle adhesion.

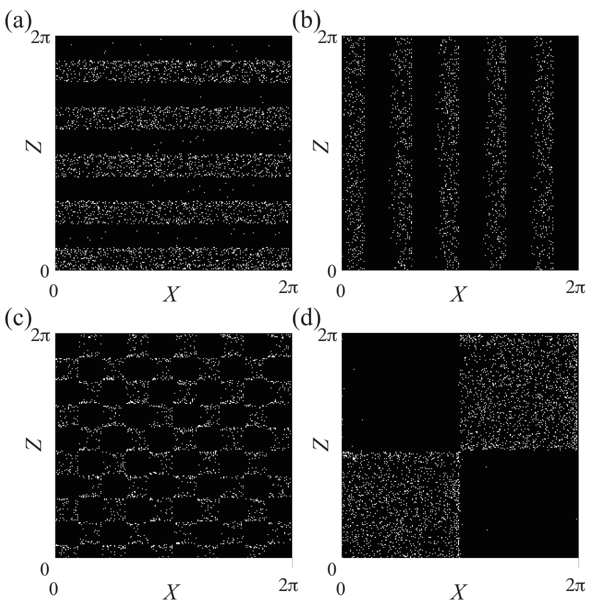

Figure 7. The accumulated adhered-particle on the wall at $0 < t < 80$. The white dot means a single adhered particle: (a) Case 1, (b) Case 2, (c) Case 3, and (d) Case 4.

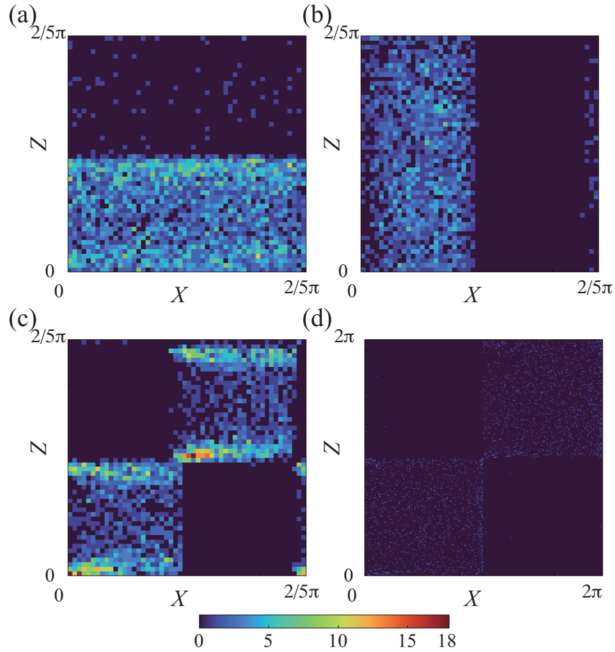

Figure 8. The ratio of the local number of attachments to the total number of attachments: (a) Case 1, (b) Case 2, (c) Case 3, and (d) Case 4.

REFERENCES

Choi, C. M. & Kim, C. J. 2006 Large slip of aqueous liquid flow over a nanoengineered superhydrophobic surface. *Physical Review Letters* **96** (066001).

Daniello, R. J., Waterhouse N. E. & Rothstein J. P. 2009 Drag reduction in turbulent flows over superhydrophobic surfaces. *Physics of Fluids* **21** (085103).

Ham, F. E., Lien F. S. & Strong A. B. 2002 A fully conservative second- order finite difference scheme for incompressible flow on nonuniform grids. *Journal of Computational Physics* (177), 117–133.

Hasegawa, Y., Frohnapfel B. & Kasagi N. 2011 Effects of spatially varying slip length on friction drag reduction in wall turbulence. *Journal of Physics* **318** (022028).

Kim, J., Moin P. & Moser R. 1987 Turbulence statistics in fully developed channel flow at low reynolds number. *Journal of Fluid Mechanics* **177**, 133–166.

Martell, B. M., Perot J. B. & Rothstein J. P. 2009 Direct numerical simulations of turbulent flows over superhydrophobic surfaces. *Journal of Fluid Mechanics* **620**, 31–41.

Spalarta, P. R., Mosera R. D. & Rogers M. M. 1991 Spectral methods for the navier-stokes equations with one infinite and two periodic directions. *Journal of Computational Physics* **96**, 297–324.

Watanabe, S., Mamori H. & Fukagata K. 2017 Drag-reducing performance of obliquely aligned superhydrophobic surface in turbulent channel flow. *Fluid Dynamics Research* **49** (025501), 20.